Bioactive Materials 23 (2023) 383–393

Contents lists available at ScienceDirect

Bioactive Materials

journal homepage: www.keaipublishing.com/en/journals/bioactive-materials

Real-time and label-free biosensing using moiré pattern generated by bioresponsive hydrogel

Semin Kim [a,1], Geehong Kim [b,1], Yong Woo Ji [c,d,1], Chae-Eun Moon [d,e], Yuna Jung [a], Hyung Keun Lee [d,f,g,***], JaeJong Lee [b,h,**], Won-Gun Koh [a,*]

[a] Department of Chemical and Biomolecular Engineering, Yonsei University, 50 Yonsei-ro, Seodaemun-gu, Seoul, 120-749, Republic of Korea
[b] Korea Institute of Machinery & Materials, Nano-Convergence Mechanical Systems Research Division, 156 Gajeongbuk-ro, Yuseong-gu, Daejeon, 34103, Republic of Korea
[c] Department of Ophthalmology, Yongin Severance Hospital, Yonsei University College of Medicine, 363, Dongbaekjukjeon-daero, Giheung-gu, Yongin-si, Gyeonggi-do, 16995, Republic of Korea
[d] Institute of Vision Research, Department of Ophthalmology, Yonsei University College of Medicine, 50-1 Yonsei-ro, Seodaemun-gu, Seoul, 120-749, Republic of Korea
[e] Department of Ophthalmology, Graduate School of Medical Science, Brain Korea 21 Project, Yonsei University College of Medicine, Republic of Korea
[f] College of Pharmacy, Yonsei University, 85 Songdo Hwawak-ro, Yeonsu-gu, Incheon, 26426, Republic of Korea
[g] Department of Ophthalmology, Gangnam Severance Hospital, Yonsei University College of Medicine, 211 Eonju-ro, Gangnam-gu, Seoul, 06273, Republic of Korea
[h] Department of Nanomechatronics, University of Science and Technology, 217, Gajeong-ro, Yuseong-gu, Daejeon 34113, Republic of Korea

ARTICLE INFO

Keywords:
Bioresponsive hydrogel
Moiré pattern
Biosensing
Intraocular lens
Aqueous humor

ABSTRACT

Bioresponsive hydrogels are smart materials that respond to various external stimuli and exhibit great potential as biosensors owing to their capability of real-time and label-free detection. Here, we propose a sensing platform based on bioresponsive hydrogels, employing the concept of moiré patterns. Two sets of line patterns with different pitch sizes are prepared; a hydrogel grating whose pitch size changes according to external stimuli and a reference grating with constant pitch size. The volume changes of the hydrogel caused by external stimuli changes the pitch size of the hydrogel grating, and subsequently, the pitch sizes of the moiré patterns (moiré signal), whose values can be obtained in a real-time and label-free manner through customized moiré microscopy and signal processing. After confirming that the pH-induced swelling of hydrogel could be monitored using moiré patterns, we performed moiré pattern-based detection of specific proteins using protein-responsive hydrogel that underwent shrinking via interaction with target proteins. Brain-derived neurotrophic factor and platelet-derived growth factor were selected as the model proteins, and our proposed system successfully detected both proteins at nanomolar levels. In both cases, the pitch size change of hydrogel grating was monitored much more sensitively using moiré patterns than through direct measurements. The changes in the moiré signals caused by target proteins were detected in *ex-vivo* environments using a custom-made intraocular lens incorporating the hydrogel grating, demonstrating the capability of the proposed system to detect various markers in intraocular aqueous humor, when implanted in the eye.

1. Introduction

Many studies are being conducted on bioresponsive hydrogels that are useful in a variety of biomedical applications such as biosensing [1–3], controlled drug delivery [4–6], and tissue engineering [7–9], because of their specific responses to various external stimuli. Generally,

Peer review under responsibility of KeAi Communications Co., Ltd.

* Corresponding author. Department of Chemical and Biomolecular Engineering, Yonsei University, 50 Yonsei-ro, Seodaemun-gu, Seoul 120-749, Republic of Korea.

** Corresponding author. Korea Institute of Machinery & Materials, Nano-Convergence Mechanical Systems Research Division, 156 Gajeongbuk-ro, Yuseong-gu, Daejeon, 34103, Republic of Korea.

*** Corresponding author. Institute of Vascular Disease and Metabolism, Yonsei University College of Medicine, 211 Eonju-ro, Gangnam-gu, Seoul, 06273, Republic of Korea.

E-mail addresses: shadik@yuhs.ac (H.K. Lee), jjlee@kimm.re.kr (J. Lee), wongun@yonsei.ac.kr (W.-G. Koh).

[1] These authors contributed equally.

https://doi.org/10.1016/j.bioactmat.2022.11.010
Received 5 July 2022; Received in revised form 14 October 2022; Accepted 15 November 2022

bioresponsive hydrogels undergo swelling/shrinking or sol–gel transitions in response to physical (temperature, electric or magnetic fields, and mechanical stress) [10–13] or chemical (pH, metal ions, and other chemical molecules) stimuli [14–16].

Biosensing is an obvious and important application of bioresponsive hydrogels as it allows label-free detection through simple readout techniques. In biosensors, various biological recognition events such as antigen-antibody binding [12,17], DNA hybridization [18–21], or target-aptamer or enzyme-substrate interactions [22,23], induce macroscopically observable changes in the hydrogel properties. Usually, the interactions between receptors immobilized in the hydrogel and targets diffusing into the hydrogel induce physical changes in the volume or length of the hydrogel owing to the change in crosslinking density [12,13]. Various techniques have been used to quantify these target-responsive hydrogel transitions for sensing specific biomolecules such as glucose or proteins [24–26].

When using bioresponsive hydrogels for biosensing, the simplest detection method is to directly measure the change in the hydrogel size in terms of the swelling/shrinking percentage. Shoemaker et al. [27] and Miyata et al. [1,13] prepared bioresponsive hydrogels that underwent volume changes owing to the formation of glucose/Con A or antigen/antibody complexes. The diffusion of glucose or antigen into the sample solution disrupted the pre-existing noncovalent crosslinks, causing the swelling of the hydrogel, which facilitated the quantitative analysis of the amount of glucose or target protein in the sample solutions. In other studies, receptor-incorporated or molecular imprinted hydrogels were prepared, which could form noncovalent crosslinks with targets and undergo different degrees of shrinkage depending on the target concentration [28,29]. In addition to binding events between bioreceptors and targets, enzymatic cleavage could also be utilized in the sensing mechanisms of bioresponsive hydrogels. Enzyme-specific peptides were used as crosslinkers of hydrogels to enable the target enzymes to diffuse into the hydrogel and break the peptides [30]. These enzyme-substrate reactions decreased the crosslinking density of the hydrogel, which caused swelling or gel-to-sol transition of the hydrogel. Physical changes of the hydrogels have also been induced by the conformational changes in proteins that happen during ligand-binding events [31,32].

However, the direct measurement of hydrogel size is neither accurate nor sensitive, which might result in different results depending on the person and require many receptor molecules. Therefore, much effort has been made to incorporate other sensing modalities into bioresponsive hydrogels to provide easily detectable readouts of the physical changes in the hydrogel. Optical responses such as changes of fluorescence intensity (using fluorescence molecules) or diffraction wavelength (using hydrogel photonic crystals) have been used as output signals [33,34]. Another sensor with an optical output signal has been fabricated using microlenses [35,36]. Swelling or shrinking of the hydrogel causes changes in the local radius of curvature or refractive index, which subsequently changes the optical properties of the microlenses. More recently, bioresponsive hydrogels were combined with diffraction gratings and/or SPR analysis for the label-free detection of specific targets [37–39].

In the present study, for the first time, we employ the concept of moiré patterns to detect target proteins using bioresponsive hydrogels. A moiré pattern or moiré fringe is an interference pattern formed by overlapping similar but slightly offset templates, as shown in Scheme 1a. For the formation of moiré interference pattern, the two patterns should not be identical; instead, they should be rotated, displaced, or have slightly different pitches [40–43]. In this study, a moiré pattern is produced by overlapping hydrogel and reference gratings with different pitch sizes. The resulting moiré patterns are quantitatively monitored using a customized moiré optical microscope. When the pitch size of the hydrogel grating changes by the volume change of the hydrogel caused by external stimuli, the pitch size of the moiré pattern (moiré signal) also changes, as shown in Scheme 1b. The moiré pattern facilitates easier signal readout and more sensitive detection than the direct measurement of physical changes in the hydrogel, such as size or crosslinking density. After confirming that the pH-dependent swelling of pH-responsive hydrogels can be successfully monitored using moiré patterns, we prepared a protein-responsive hydrogel by incorporating antibodies into the hydrogel network. The diffusion of target proteins into the hydrogel and their subsequent binding to the corresponding antibodies produce additional crosslinks in the hydrogel, shrinking the

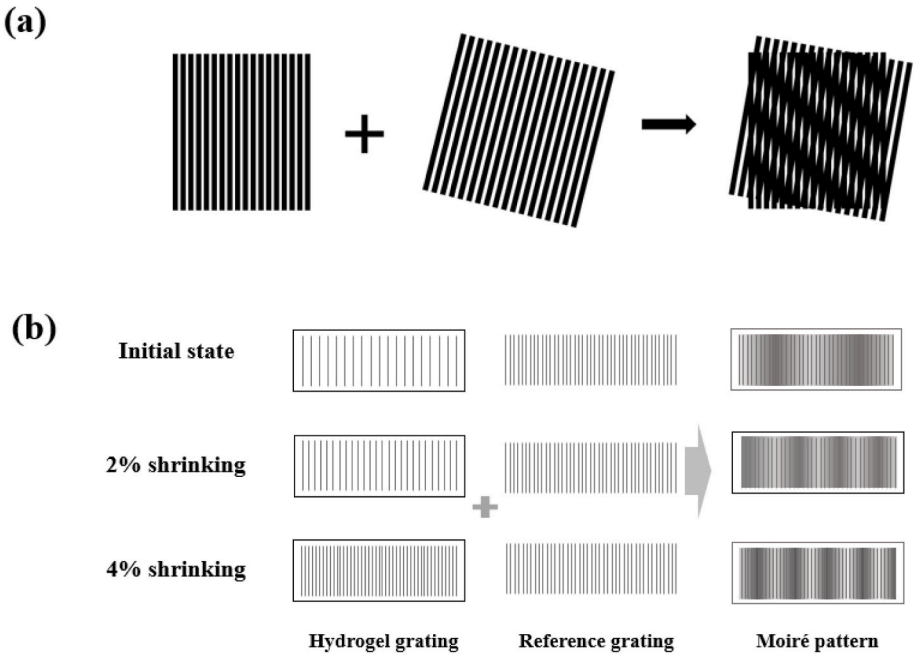

Scheme 1. Use of moiré patterns to monitor the volume change of bioresponsive hydrogels. (a) An example of moiré pattern produced by two sets of line patterns, one set inclined at a certain angle to the other. (b) Schematic illustration showing the moiré patterns formed by overlaying the reference grating and hydrogel grating with different.

hydrogel. The concentration-dependent change in the hydrogel volume is monitored using a moiré pattern. After confirming the capability of target-protein detection, an intraocular lens (IOL) containing a hydrogel grating was prepared and implanted in porcine eyes, as a proof of concept for the potential application of the proposed sensing system to the detection of various markers in intraocular aqueous humor (AH). Target-responsive hydrogel shrinking was successfully monitored with a moiré pattern in *ex-vivo* environments.

2. Materials and methods

2.1. Materials

Acrylic acid (AA), acrylamide (AAm), ammonium persulfate (APS), N′, N′-methylenebisacrylamide (MBAA), poly (vinyl alcohol) (MW 9000–10000), 2-hydroxyethyl methacrylate (HEMA), ethylene glycol diacrylate (EGDA), 2-hydroxy-2-methylpropiophnone (HOMPP), N, N, N′, N′-tetramethyl-ethylenediamine (TEMED), and bovine serum albumin (BSA) were purchased from Sigma Aldrich (Milwaukee, WI, USA). Phosphate buffer saline (PBS; pH 7.4, 1X), Alexa Fluor 647 protein labeling kit, dialysis cassettes (MWCO 2000, 0.2–0.5 mL), and carbonate-bicarbonate buffer packs were purchased from Thermofisher Ltd. (Waltham, MA, USA). N-succinimidyl acrylate (NSA) was purchased from Tokyo Chemical Industry Co., Ltd. (Tokyo, Japan). Balanced salt solution (BSS) was purchased from Alcon Laboratories, Inc. (South Freeway FortWorth, TX, USA). Sulfuric acid (H_2SO_4) and hydrogen peroxide (H_2O_2) were purchased from Ducksan Co., Ltd. (Ansan, Korea). pH buffer solutions (pH 4, 6, and 7) were purchased from SAMCHUN Chemical Co., Ltd. (Seoul, Korea). Anti-BDNF, BDNF protein, anti-PDGF, and PDGF protein, FITC-anti-BDNF were purchased from PEPROTECH Inc. (Rocky Hill, NJ, USA). SU-8 50 and SU-8 Developer were purchased from MICROCHEM. (Round Rock, TX, USA). SYLGARD 184 silicon elastomer base (PDMS prepolymer) and SYLGARD 184 silicon elastomer curing agent (curing agent) were purchased from DOW Chemical Company (Midland, MI, USA). EPIBOND (protein bond) was purchased from DOOWON MEDITEC Co., Ltd. (Yongin, Korea).

2.2. Preparation of microgroove-patterned hydrogel grating

Hydrogel gratings were prepared via replica molding using a microgroove-patterned silicon wafer as the mold. To fabricate a microgroove-patterned silicon wafer with a 500 nm oxide layer, a microgroove pattern with a pitch size of 16 μm (widths of both the ridge and grooves in the hydrogel grating were 8 μm) and depth of 1 μm was first generated through photolithography followed by ion etching, as described in a previous study [44]. Each hydrogel precursor solution was poured onto a silicon mold and crosslinked to produce a microgroove-patterned hydrogel replica (hydrogel grating). After detaching the crosslinked hydrogel from the silicon mold, freestanding hydrogel gratings were obtained.

2.2.1. Synthesis of pH-responsive hydrogel grating

Thermal crosslinking was used to prepare the pH-responsive hydrogel gratings. The hydrogel precursor solution was composed of AAm (4.92 mmol), AA (2.08 mmol), and MBAA (0.1 mmol) dissolved in 342 μL of DI water, to which 8 μL of 10 wt% APS was added. This hydrogel precursor solution was dropped onto a silicon wafer mold with a pitch size of 16 μm. After placing the cover glass on the precursor solution, thermal crosslinking was performed at 80 °C for 1 h. The resultant 1 mm-thick pH-responsive hydrogel was detached from the silicon wafer and washed with DI water for one day to remove any unreacted material.

2.2.2. Synthesis of protein-responsive hydrogel grating

The control hydrogel grating without antibodies was fabricated as follows: AAm (0.211 mmol) and MBAA (0.0065 mmol) were dissolved in 97 μL of PBS, following which 2.5 μL of 10 wt% APS and 0.5 μL of TEMED were sequentially added and vortexed for 1 s. The resultant hydrogel precursor solution was dropped onto a silicon wafer mold with a pitch size of 16 μm, covered with a cover glass, and polymerized at 25 °C to prepare a control hydrogel grating with a thickness of 1 mm. Hydrogel gratings responsive to target proteins such as BDNF and PDGF were prepared as follows. Antibody and NSA solutions were prepared at concentrations of 1 and 0.4 mg/mL, respectively. The antibody solution was added to the NSA solution such that the molar ratio of antibody to NSA was 1:6 and total volume was 45 μL. The reaction between the antibody and NSA proceeded for 3 h at 25 °C, synthesizing the acylated antibody according to the Shoemaker method [27]. To remove the unreacted NSA, dialysis was performed for one day using a 2000 MWCO dialysis kit. AAm (0.211 mmol) and MBAA (0.0065 mmol) were dissolved in 52 μL of PBS, to which 45 μL of the acylated antibody solution was added. Thereafter, 2.5 μL of 10 wt% APS and 0.5 μL of TEMED were sequentially added and vortexed for 1 s. The hydrogel precursor solution was dropped onto a silicon wafer mold with a pitch size of 16 μm, covered with a cover glass, and polymerized at 25 °C to prepare protein-responsive hydrogels with a thickness of 1 mm. The hydrogels were washed with DI water for one day to remove any unreacted material. The amount of antibodies conjugated to the responsive hydrogel grating was indirectly estimated using fluorescence method as described in the previous study [28]. In this study, FITC-labeled anti-BDNF (FITC-anti-BDNF) was used for quantification. Approximately 0.406 mg/mL (893.29 nM) was bound to the responsive hydrogel. Considering that 1 mg/mL (2200 nM) of anti-BDNF was initially used from the initial conjugation process, 40 wt% of anti-BDNF was conjugated within the responsive hydrogel.

2.3. Fluorescence analysis of protein recognition

The copolymerization of the acylate antibody and AAm during the synthesis of protein-responsive hydrogels generated pendant antibodies on the hydrogel networks. To confirm the binding capabilities of the pendant antibodies to the target proteins, BDNF-responsive hydrogels conjugated with anti-BDNF were reacted with fluorescence-labeled BDNF. BDNF (111 nM) was labeled with Alexa Fluor 647 dye (Alexa dye) according to the supplier's protocol to produce BDNF-Alexa. The BDNF-responsive hydrogel was then incubated with BDNF-Alexa for 2 h. For comparison, the control hydrogel and BDNF-responsive hydrogel were also reacted with BDNF-Alexa and Alexa dye, respectively, for 2 h. After 2 h of incubation with the fluorescence solutions, the hydrogels were observed using a fluorescence microscope (Carl Zeiss Inc. Thornwood, NY, USA). The fluorescence intensities of the hydrogels were obtained using image analysis software (KS 300, Carl Zeiss Inc.). Then, the three hydrogels were washed in DI water for 24 h to allow the unbound fluorescence molecules (BDNF-Alexa and free Alexa dye) to diffuse out from the hydrogel. After washing, the hydrogels were observed using a fluorescence microscope.

2.4. Pt coating and TGA study

The control hydrogel and pH- or protein-responsive hydrogel gratings were coated with Pt using a Pt coater (CRESSINGTON Scientific Instruments Ltd., Chalk Hill, Watford, UK) for 200 s at 3 cm from the Pt source at a current of 10 mA. Pt-coating was used as a contrast agent for better visualization of moiré signals from the hydrogel grating. Prior to Pt coating, each hydrogel was fully dried and reswollen after sputtering. The surfaces morphology and atomic percentage of the hydrogel gratings before and after Pt coating were observed using a SEM equipped with energy-dispersive X-ray spectroscopy (EDS) (JEOL-7610F-Plus instrument at 10 kV, JEOL Co., Tokyo, Japan). The chemical properties of Pt-coated hydrogel gratings were investigated by X-ray photoelectron spectroscopy (XPS) (K-alpha, Thermo, UK). TGA (TA Instruments, New Castle, DE, USA) was performed on the dried hydrogel samples, at a

heating rate of 10 °C/min in N_2 atmosphere, to measure the amount of Pt coated on each hydrogel.

2.5. Moiré microscopy system and signal processing

To produce moiré signals, the reference gratings were overlaid with the hydrogel gratings. When the pitch size of the hydrogel grating changed because of the volume change of the hydrogel by external stimuli, moiré signal also changed. The pitch sizes of the reference gratings for the pH-responsive and protein-responsive hydrogel sensing modules were 58 and 43 μm, respectively, which were determined by the fact that the pH-induced volume change was greater than the protein-induced volume change of the hydrogel.

Image acquisition and signal processing were performed using the moiré microscope system shown in Fig. 1a. Reference grating was fabricated on the glass substrate, where chrome patterns were generated using photolithography (Fig. S1 in Supplementary Data). Pattern-containing glass substrate was diced according to the size to be used and inserted between the light source and projection lens. The image of the reference grating, which was obtained when light from the source passed through the reference grating, projection lens, beam splitter, and objective lens, was overlaid with the hydrogel gratings at a magnification of 0.438 × . The image of the resultant moiré pattern could be observed in real time on the monitor using a CCD camera, as shown in Fig. 1b. The moiré pattern was processed using a fast Fourier transform that converted the spatial domain on the x-axis into the frequency domain. An example of moiré pattern processing is presented in Fig. 1b. When the users dragged a line at a selected location on the screen, the output intensity profile was recorded as a sinusoidal waveform at the lower-left corner (solid rectangular line) of the monitor. When this wave was subjected to fast Fourier transformation, the frequency components of the various waves, including the moiré pattern, were displayed at the lower right corner (dotted rectangular line). The several peaks represented the frequency strengths of the moiré pattern, hydrogel grating, and reference grating. The reciprocal values of the frequency were the pitch sizes of each pattern. Among the many peaks, a signal corresponding to the moiré pattern was selected, with a size similar to the theoretical pitch size of the moiré pattern calculated by the pitch size of the reference and hydrogel gratings. The detailed method to obtain moiré signal is described in Supplementary Data with Fig. S2. In this study, the angle between hydrogel and reference grating (θ) was set as close to 0° as possible.

2.6. Cytocompatibility test using MTT assay

The cytotoxicity of prepared hydrogel was assessed against cornea endothelial cells (CEC) by measuring the cell growth using MTT (3, 4, 5-dimethylthiazol-2-yl)-2–5-diphenyltetrazolium bromide) assay according to standard protocol [45]. Bos Taurus CEC line, BCE C/D1b obtained from ATCC®, were cultivated in Dulbecco's Modified Eagle's Medium (DMEM) supplemented with 10% fetal bovine serum (FBS) and 1% antibiotic-antimycotic (Gibco®, Life Technologies, Grand Island, NY, USA). CEC cells (1 × 104 cells/well) were seeded into 96-well plate and incubated at 37 °C under 5% CO2 for 24 h. Then, the culture medium was replaced with 100 μL of complete growth medium containing the supernatant of hydrogel dispersed in the media for 1, 3, and 5 days, and incubated for 24 h. Subsequently, the incubated cells were treated with 0.5 mg/ml of MTT solution (ThermoFisher, Carlsbad, CA, M6494) diluted in serum-free media, and incubated for a further 2 h at 37 °C. The MTT solution was discarded carefully and a volume of 100 μL DMSO was added to each well. The plates were then agitated for 15 min to dissolve remaining formazan crystals completely. After 5 min of shaking, the optical density (O.D.) were determined at 570 nm using a microplate reader (TECAN, Infinite 200 pro M nano).

2.7. Ex-vivo experiments

For *ex-vivo* experiments, hydrogel gratings were inserted into custom-made PHEMA-based IOL supports, which were fabricated using PDMS molds prepared using a conventional replica molding process. Briefly, a Si master containing replica patterns of the PDMS mold was fabricated using SU-8 50 via spin coating, prebaking, UV exposure, postbaking, and developing processes. The design and dimensions of the PDMS mold are shown in Fig. S3a in Supplementary Data. The mold was designed such that the resultant IOL had two holes: one for the target-responsive hydrogel grating and the other for the control hydrogel grating without pendant antibodies. The resulting IOL-shaped PDMS mold was filled with 80 μL of precursor solution consisting of 77.2 μL of HEMA, 2 μL of EGDA, and 0.8 μL of HOMPP, covered with a PDMS membrane and cured by UV exposure (365 nm, 5300 mW/cm^2, EXFO OmniCure Series 1000, UV spot lamp, Mississauga, Ontario, Canada) for 280 s. Disk-shaped control and protein-responsive hydrogel gratings with a diameter of 2 mm were inserted into each hole, using a protein bond to complete the hydrogel grating–loaded IOL (Fig. S3b in Supplementary Data).

Fresh porcine eyes were obtained from a local butcher and dissected prior to remove the pig's hair using hot steam. After the eyeballs were immediately transferred to the laboratory in a thermal bag, *ex-vivo* experiments were performed. Five porcine eyes were implanted with hydrogel grating-loaded IOLs. The surgical procedure was carried out by a single experienced surgeon (Y. W. Ji). Briefly, a 4 mm sized clear cornea limbal incision was generated, and the anterior chamber was

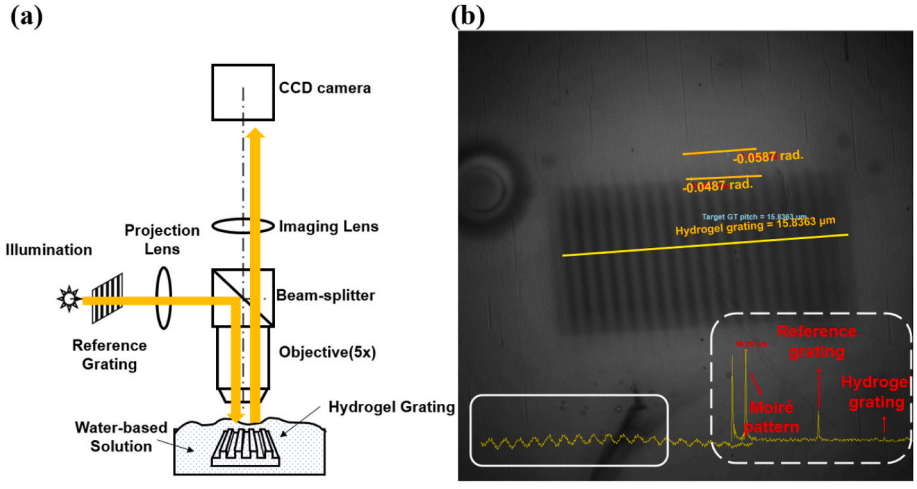

Fig. 1. Acquisition of moiré pattern image and quantitative signal using custom-made moiré microscopy system. (a) Components and working mechanism of moiré microscopy system. (b) Image of moiré pattern and the result of signal processing to obtain the pitch size of the moiré pattern. Solid rectangular line represents output signals containing various patterns recorded as multi-waveforms and dotted line represents intensity of pitch size of various patterns including the moiré pattern obtained by fast Fourier transformation.

filled with an ophthalmic viscosurgical device (OVD) (Healon, Alcon, Fort Worth, Texas, USA). The IOL was inserted into the anterior chamber and the OVD was replaced with BSS. The corneal wound was closed using interrupted 10–0 nylon sutures.

3. Results and discussion

3.1. Formation of moiré pattern with hydrogel grating

In this study, a moiré pattern was produced by overlapping hydrogel and reference gratings. Photocrosslinking of the hydrogel precursor solution on a silicon wafer mold produced a hydrogel grating with aligned microgrooves. When a non-responsive PAAm-based control hydrogel grating was prepared, the widths of the grooves and ridge of the microgroove-patterned hydrogel right after photocrosslinking were 9.1 and 7.2 μm (pitch size: 16.3 μm), respectively, as shown in Fig. 2a. Considering the dimensions of the microgroove pattern on a silicon wafer mold (8 μm groove and 8 μm ridge), it was confirmed that the microgroove structures were successfully replicated from the silicon mold. The fabrication of the hydrogel grating was further confirmed using an SEM, which showed clearly aligned microgroove patterns on the hydrogel grating. Because fully dried hydrogel gratings were used in the SEM analysis (Fig. 2b and Fig. S4a in Supplementary Data), the widths of the groove and ridge (3.2 and 4.6 μm, respectively) were significantly decreased (in the dry state), owing to the high-water content of the PAAm hydrogel.

When the resultant microgroove-patterned hydrogel was placed in a moiré microscopy system with a reference grating (pitch size: 43 μm), no moiré signal was observed. Because the transparent hydrogel had a refractive index (1.34) similar to that of water (1.33) [46], the presence of water between the hydrogel and reference grating prevented the formation of a moiré pattern. To solve this problem, the hydrogel surface was coated with Pt which is well-known for its biocompatibility. Although the Pt-coated hydrogel grating had a rougher surface than that of the bare hydrogel grating, the microgroove patterns were well-maintained, as shown in Fig. 2c and Fig. S4b in Supplementary Data. The Pt coating was further confirmed through TGA (Fig. 2d). Because TGA was carried out under N_2 atmosphere, the remaining weight of the bare hydrogel could be attributed to the charred organic leftovers, and the difference in weight between the bare and Pt-coated hydrogels could be attributed to the amount of coated Pt. For both hydrogels, a preliminary mass loss (approximately 30%) was observed during the decomposition of water and air. A subsequent loss occurred at around 380 °C because of the decomposition of PAAm. The mass loss continued until only 12.6% and 16.0% of the initial mass remained for the bare and Pt-coated hydrogels, respectively. This difference arose from the presence of the Pt coating on the hydrogel. TGA analysis also indicates that there was no significant loss of Pt-coating even after hydrogel underwent swelling in aqueous environment as demonstrated in Fig. S5 in Supplementary Data. SEM-EDS and XPS analysis was performed for more quantitative analysis of Pt-coating on the hydrogel grating. As shown in the SEM-EDS analysis (Fig. S6a in Supplementary Data), a high amount of Pt was observed after Pt-coating, and the Pt was homogenously distributed on the surfaces of the hydrogel grating. In contrast, no Pt was detected in the SEM-EDS images of the bare hydrogel grating. Similar results could be obtained from XPS study (Fig. S6b in Supplementary Data). XPS spectra for Pt4f clearly shows the presence of Pt after coating process, while no Pt was observed bare hydrogel grating. The water content of the Pt-coated hydrogel and the swelling kinetics were compared with those of the bare hydrogel, and the results are presented in Fig. 2e. The results indicate that Pt coating does not affect the water absorption capacity of the hydrogel but slows down the diffusion kinetics of water through the hydrogel. After Pt coating, the moiré pattern was visible, as shown in Fig. 2f. When a line was drawn on the selected region of the moiré pattern, the pitch size corresponding to the moiré pattern (moiré signal) could be obtained via signal processing. Therefore, Pt-coating was used as a contrast agent for better visualization of moiré signals from the hydrogel grating in our study.

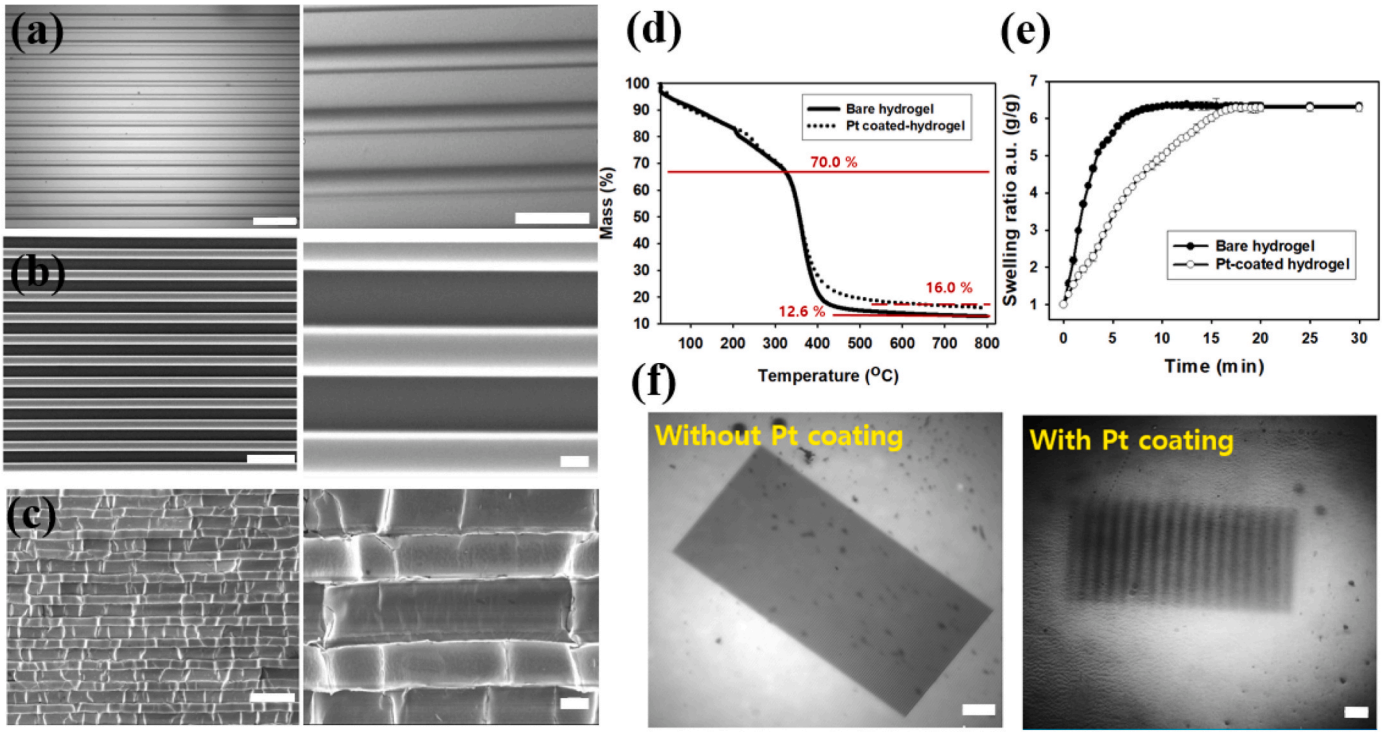

Fig. 2. Preparation of hydrogel grating with microgroove patterns. (a) Optical image of hydrogel grating obtained right after photo-crosslinking. Scale bar: 40 μm (left) and 20 μm (right). (b) SEM images of hydrogel grating. (c) SEM images of Pt-coated hydrogel grating. In (b)–(c), Scale bars: 10 μm (left) and 1 μm (right). (d) TGA analysis of bare and Pt-coated hydrogel grating. (e) Water absorption behavior of bare and Pt-coated hydrogel grating. (f) Moiré patterns formed by overlaying reference grating on the bare hydrogel grating or Pt-coated hydrogel grating. Scale bar: 100 μm.

3.2. Monitoring pH change using moiré signal

After confirming that the Pt-coated hydrogel grating could generate moiré signals with a reference grating, we first investigated the capability of our proposed system to monitor the properties of the external environment, such as the pH. For this, a pH-sensitive hydrogel grating was prepared by adding AA to the hydrogel precursor solution and synthesizing a copolymer hydrogel consisting of PAA and PAAm. Because PAA undergoes different levels of swelling depending on the pH due to the ionization of the carboxyl group above its pK_a (4.7), a pH change in the solution was expected to alter the pitch size of the hydrogel grating. To monitor the change in the moiré signals caused by a pH-induced volume change of the hydrogel, the pH-responsive hydrogel gratings were placed in pH 4 and pH 7 buffers. Moiré patterns were observed, and subsequently, moiré signals were obtained as shown in Fig. 3a and **b**. At pH 4, there was a slight increase in the moiré signal (89.25 μm → 97.61 μm), resulting from a small change in the volume of the hydrogel because little ionization occurred below the pK_a of PAA. However, at pH 7, there was a significant change in the moiré signal (89.47 μm → 328.59 μm) because the PAA became charged and swelled above the pK_a value. To investigate the quantitative pH-sensing capability of the proposed system, the time-dependent change of the moiré signal was investigated at three different pH (pH 4, 6, and 7). pH 4 and 6 was chosen considering the pKa value (4.7) of PAA which was used as pH-responsive hydrogel, while pH 7 was chosen considering the pH of aqueous humor in human [47,48]. As shown in Fig. 3c, the values of the moiré signal could be obtained in real-time. As the reaction time and pH increased, the moiré signal increased because the carboxyl groups in PAA released more protons and became COO^-, which caused hydrogel swelling because of the increased repulsion between COO^- and greater bonding with H_2O. The most important advantage of using a moiré pattern, when compared to the direct measurement of volume or length change, is the signal amplification. Fig. 3d shows a comparison of the pitch sizes of the moiré pattern and hydrogel grating. After 95 min incubation in pH 7 buffer, the pitch size of the hydrogel sensing module increased by approximately 20%, whereas that of the moiré signal increased by more than 260%. Signal amplification by the moiré pattern can be understood from a well-known formula. According to Eq. (5) in Supplementary Data, 19.2% increase in the pitch size of the hydrogel grating (P_H), from 19.75 to 23.55 μm, resulted in a 263.7% change in P_M, from 88.73 to 322.69 μm at pH 7 when the angle θ between the reference and hydrogel grating grids was set to 0°.

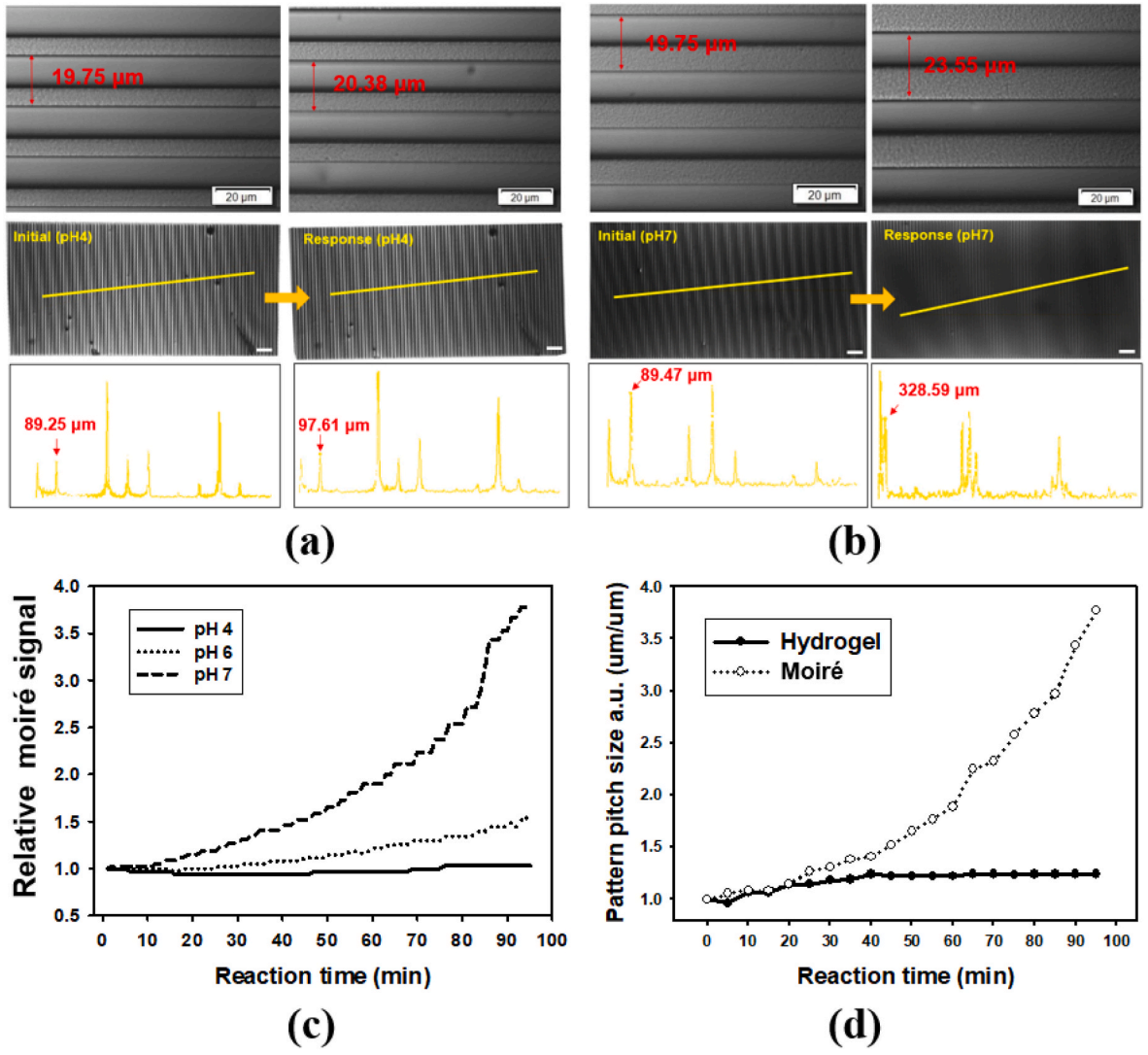

Fig. 3. Monitoring pH-responsiveness of hydrogel grating using moiré patterns. pH-dependent swelling of hydrogel grating and subsequent change of moiré signal (a) in pH 4 buffer solution and (b) in pH 7 buffer solution. Optical image of hydrogel grating (top), optical images of moiré patterns (middle) (The yellow line was drawn to be perpendicular to the moiré pattern.), and moiré signals obtained from reference and hydrogel gratings (bottom). Scale bar: 100 μm. (c) Quantitative analysis of moiré signal as a function of pH and time. (d) Comparison of pitch size change between moiré pattern and hydrogel grating.

3.3. Synthesis of hydrogel gratings responsive to target proteins

To prepare protein-responsive hydrogels, antibodies against the target proteins were modified with a polymerizable acrylate terminus. Copolymerization of the acylated antibodies and AAm with an initiator, crosslinker, and catalyst on the silicon wafer mold, and the subsequent Pt coating produced a hydrogel grating responsive to target proteins, as shown in Fig. 4a. Diffusion of the target proteins into a hydrogel increased the degree of crosslinking of the hydrogel network via the formation of antigen–antibody complexes, resulting in the shrinking of the hydrogel.

Prior to investigating the capability of the hydrogel grating to detect target proteins using a moiré pattern, its capacity to recognize a specific target protein using pendant antibodies was confirmed using the fluorescence method. For this, hydrogels incorporating antibodies (anti-BDNF) or control PAAm hydrogels without antibodies were prepared, which were then reacted with fluorescence-labeled BDNF (BDNF-Alexa) or Alexa Fluor 647 dye (Alexa dye). Three different combinations were prepared: (i) control PAAm-based hydrogel reacted with BDNF-Alexa, (ii) antibody-incorporated hydrogel reacted with BDNF-Alexa, and (iii) antibody-incorporated hydrogel reacted with Alexa dye. After 2 h of incubation, all the hydrogels emitted strong red fluorescence owing to the diffusion of BDNF-Alexa or Alexa dye into the hydrogel (Fig. 4b). Although the molecular weight of BDNF-Alexa was much greater than that of the Alexa dye, 2 h were a sufficient duration for both molecules to diffuse and occupy the free volume in the hydrogel. The three hydrogels emitted almost the same fluorescence intensity. However, after washing with DI water for 24 h, each hydrogel exhibited a different fluorescence intensity (Fig. 4c). No fluorescence was detected in the control hydrogel reacted with BDNF-Alexa and the antibody-incorporated hydrogel reacted with Alexa dye because both fluorescence molecules were physically entrapped within the hydrogel, and consequently, easily removed from the hydrogel by washing. In contrast, the antibody-incorporated hydrogel that reacted with BDNF-Alexa maintained the fluorescence after 24 h of washing, owing to the binding of the fluorescent BDNF to anti-BDNF within the hydrogel. It is worth noting that the target proteins (BDNF) were bound to antibodies within the hydrogel in a homogeneous distribution, as demonstrated by the fluorescence intensity profile shown in Fig. 4c. These results indicate that target-specific antibodies were successfully incorporated into the hydrogel via copolymerization and that the hydrogels maintained their ability to bind target proteins.

In-vitro biocompatibility testing was performed for 5 days using MTT assay for protein-responsive hydrogel grating. Fig. S7 in Supplementary Data shows that cells were viable and proliferated in the presence of protein-responsive hydrogel grating, which was similar to the cell behavior in control group. This result indicates that the Pt-coated and antibody-immobilized hydrogel grating was cytocompatible without any toxic effects.

3.4. Detection of target proteins using moiré signal

As mentioned previously, the formation of an antigen–antibody complex within the hydrogel in the presence of the target protein, decreased the pitch size of the hydrogel grating and subsequently, that of the moiré signal. Movie S1 in Supplementary Video shows the decrease of moiré signal in real time. In this case, hydrogel grating was incubated with relatively high concentration of BDNF (1.11 μM) for easier observation. To further investigate this detection mechanism, various concentration of BDNF was reacted with BDNF-responsive hydrogel gratings, and resultant change of moiré signals were monitored.

Supplementary data related to this article can be found at https://doi.org/10.1016/j.bioactmat.2022.11.010.

As shown in Fig. 5a, the hydrogel underwent shrinking owing to the binding of BDNF with the incorporated anti-BDNF, and consequently, a decreased moiré signal (93.09 μm → 80.84 μm) was observed. Fig. 5b shows the change in the pitch size of the hydrogel gratings and moiré patterns, with reaction time for the same BDNF concentration. In both cases, the pitch size decreased with the reaction time and reached a minimum after 2 h. However, the changes of pitch size in moiré pattern were much more significant than that those in hydrogel grating, confirming the signal amplification by using moiré signal. For a more quantitative analysis, the concentration- and time-dependent responses of the moiré signal to BDNF were monitored, as shown in Fig. 5c. As the concentration and reaction time increased, the change in the moiré

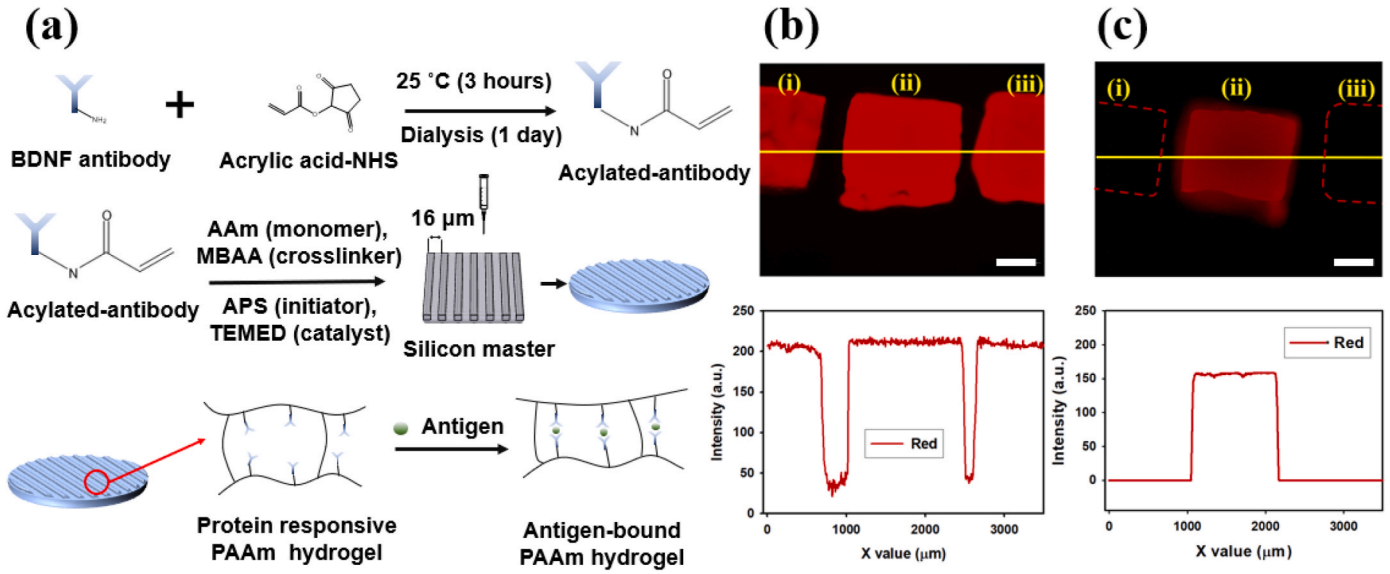

Fig. 4. Preparation of protein-responsive hydrogel grating via copolymerization of acylated antibody and AAm. (a) Schematic illustration showing preparation of acylated antibody and antibody-conjugated hydrogel grating that can undergo target protein–induced shrinking via formation of additional crosslinks by antigen–antibody complex. (b) Fluorescence images and intensity profiles of different hydrogels (BDNF-responsive and control PAAm hydrogels) incubated with BDNF-Alexa or Alexa dye for 2 h. (c) Fluorescence images and intensity profiles obtained after 24 h of washing with DI water. In Figure (b) and (c), (i) is Control PAAm hydrogel incubated with BDNF-Alexa dye, (ii) is BDNF-responsive hydrogel incubated with BDNF-Alexa dye, and (iii) is BDNF-responsive hydrogel incubated with Alexa dye. In (b)–(c), scale bar: 400 μm.

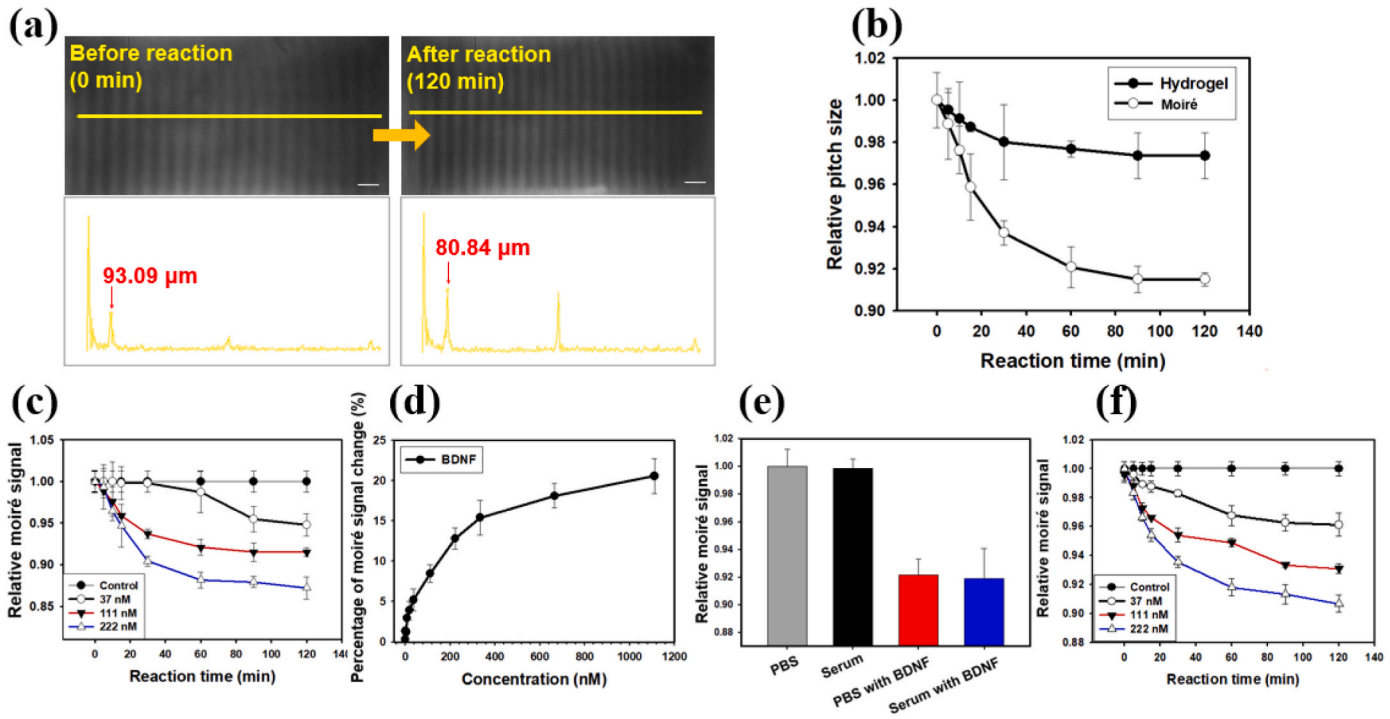

Fig. 5. Detection of target proteins using protein-responsive hydrogel grating and moiré patterns. (a) Change in pitch size of moiré pattern following the reaction between BDNF (222 nM) and BDNF-responsive hydrogel grating. Scale bar: 100 μm. (b) Comparison of pitch size change of moiré pattern and hydrogel grating when hydrogel grating is reacted with 111 nM BDNF. (c) Time-dependent change of moiré signal following the reaction with BDNF at various concentrations. (d) Increase in percentage of moiré signal as a function of BDNF concentration. (e) Selectivity experiments with BDNF-responsive hydrogel grating. (f) Time-dependent change of moiré signal following the reaction with PDGF at various concentrations.

signal increased because of the formation of more crosslinks by the binding of BDNF with anti-BDNF within the hydrogel grating. Fig. 5d shows the change in the moiré signal as a function of the BDNF concentration after reacting BDNF with the BDNF-responsive hydrogel grating for 2 h. The limit of detection (LOD) for BDNF was 29 nM. Fig. 5d shows the change in the moiré signal as a function of the BDNF concentration after reacting BDNF with the BDNF-responsive hydrogel grating for 2 h. The limit of detection (LOD) for BDNF was 29 nM. When the linear regression was performed on log (percentage of moiré signal change)(y) versus log (BDNF concentration)(x), very excellent linear relationship such as log y = 0.4315•log x+0.0468 was obtained, where R^2 is 0.9929 as shown in Fig. S8 in Supplementary Data. The selectivity was investigated by comparing the change in the moiré signal caused by the target molecule (111 nM of BDNF) in a PBS buffer with that in a serum solution. When the hydrogel gratings were reacted with pure PBS or serum, there was no change in the pitch size (Fig. 5e). However, the presence of BDNF in the PBS or serum solution decreased the moiré signal owing to the increase in the crosslinking degree of the hydrogel gratings through specific antibody–antigen binding. Importantly, the presence of various molecules in the serum solution did not have a significant effect on the change in the moiré signal; the extent of signal decrease was almost the same for BDNF in both PBS and serum solution. For further confirmation that hydrogel shrinking results from the formation of antigen-antibody complex, we investigate the effect of the amount of hydrogel-immobilized antibody on the moiré signal change. For this, we prepared protein-responsive hydrogels immobilizing different amount of antibodies (anti-BDNF), which were reacted with same concentration of target protein (111 nM of BDNF). As the concentration of immobilized antibody increased, the change in the moiré signal increased due to presence of more biding site for target that subsequently lead to more crosslinking within hydrogel (Fig. S9 in Supplementary Data). The long-term binding capacity of antibodies immobilized in hydrogel was investigated, where the BDNF-responsive hydrogel gratings that were stored in dry (in air) and wet (in PBS) condition for 7 days were reacted with 111 nM BDNF for 2 h. As shown in Fig. S10 in Supplementary Data, almost same moiré signals were observed from the BDNF-responsive hydrogel grating regardless of storage period and method.

Finally, PDGF-responsive hydrogels were prepared by incorporating anti-PDGF into the hydrogel gratings to investigate whether the proposed system could detect proteins other than BDNF. As shown in Fig. 5f, similar time- and concentration-dependent decreases in moiré signals were observed for PDGF with BDNF sensing, confirming that different target proteins could be detected using moiré signals by incorporating the corresponding antibodies into the hydrogel gratings.

These results verified that qualitative and quantitative analyses of various proteins were possible when protein-responsive hydrogels were combined with moiré signal detection systems. Although the detection was not very sensitive when compared to that of other optical detection systems such as fluorescence and surface-enhanced Raman spectroscopy (SERS), we would like to emphasize that this is the first report to amplify the sensing signal from a bioresponsive hydrogel that undergoes volume or length change, using moiré patterns. Future studies will focus on enhancing the sensing performance by optimizing the antibody incorporation into the hydrogel and the porosity of the hydrogel; the former will increase the crosslinking density of the hydrogel by allowing more antigen–antibody complex formation, and the latter will improve the diffusion of target proteins into the hydrogel sensing module.

3.5. *Detection of BDNF in ex-vivo environments*

Ex-vivo studies were performed on pig eyes to investigate the potential application of our proposed system in biosensors implantable in the eyes. Recently, biosensors using ocular lenses were developed to detect specific targets within ocular biofluids. Most of the existing studies have focused on the detection of targets within tear fluid using

contact lenses. However, from the perspective of biosensing, intraocular aqueous humor (AH) is particularly attractive because it contains various endogenous markers secreted from intraocular neural tissues. Therefore, monitoring biomolecules within the AH would allow the diagnosis of diseases related to disorders of the CNS, such as Parkinson's or Alzheimer's diseases, as well as eye diseases. Furthermore, biosensing using AH produces less signal interference than that using tears because AH is a clear and watery fluid, whereas tear is a salty fluid made up of various proteins. In addition, the implantation of an IOL into the ocular chamber filled with AH is one of the most frequently performed ocular procedures worldwide in the treatment of cataracts or presbyopia. Based on this background on AH and IOL, we hypothesized that the incorporation of a hydrogel grating into the IOL and the use of moiré signals would enable non-invasive detection of various biomarkers within the AH without invasive liquid biopsy.

An IOL containing control and target-responsive hydrogel gratings was implanted between the cornea and lens, as shown in Fig. 6a. Fig. 6b shows the IOL loaded with the control and BDNF-responsive hydrogel gratings, where microgroove patterns can be observed using a moiré microscope system. The implanted IOL was well fixed in the pig eye and visible to the naked eye (Fig. 6c). When 700 μL of 222 nM of BDNF solution in PBS was injected into one of the pig eyes, the moiré signal decreased from 152.92 to 133.80 μm in the BDNF-responsive hydrogel (Fig. 6d). Quantitative results confirmed that the decrease of moiré signal was only observed from the BDNF-responsive hydrogel, while there was no change in the case of the control hydrogel (Fig. 6e) These results confirm that the target protein (BDNF) could diffuse into the hydrogel grating inserted into the IOL and bind to the incorporated anti-BDNF, causing shrinkage of the hydrogel in *ex-vivo* environments. The initial moiré signal (152.92 μm) was different from the value obtained in the *in-vitro* experiment (93.09 μm) because the pitch size of the reference grating overlaid on the hydrogel grating was reduced by the curvature of the eyeball.

4. Conclusion

In this study, we demonstrated that the concept of moiré patterns could be successfully utilized to monitor the volume changes of bio-responsive hydrogels, caused by external stimuli. To generate a moiré pattern, a hydrogel grating with microgroove patterns was fabricated via replica molding, which was then overlaid with a reference grating with a different pitch size. Although the change in the pitch size of the hydrogel grating due to external stimuli was small, a much greater signal could be obtained when moiré signals were used. After the pH-responsiveness of the hydrogel was successfully monitored using a moiré pattern, quantitative detection of the target protein was performed using an antibody-incorporated hydrogel. The pitch size of the hydrogel grating decreased with increase in the concentration of the target proteins (BDNF and PDGF) and reaction time, which was signal amplified by the moiré pattern. Because of the specific reaction between the antigen and antibody, the resultant hydrogel gratings were selective to different target proteins, without interference from other molecules. Protein responsiveness was also visible when using the moiré pattern in *ex-vivo* environments, which opens up the possibility of using the proposed system for IOL-based detection of biomarkers within AH. Owing to its capability for real-time and label-free detection, the proposed bioresponsive hydrogel-based biosensor has great potential as an implantable sensor.

Ethics approval and consent to participate

- Our study is not related to clinical study
- Our study does not involve experimentation on animals.
- Our study does not include human subject

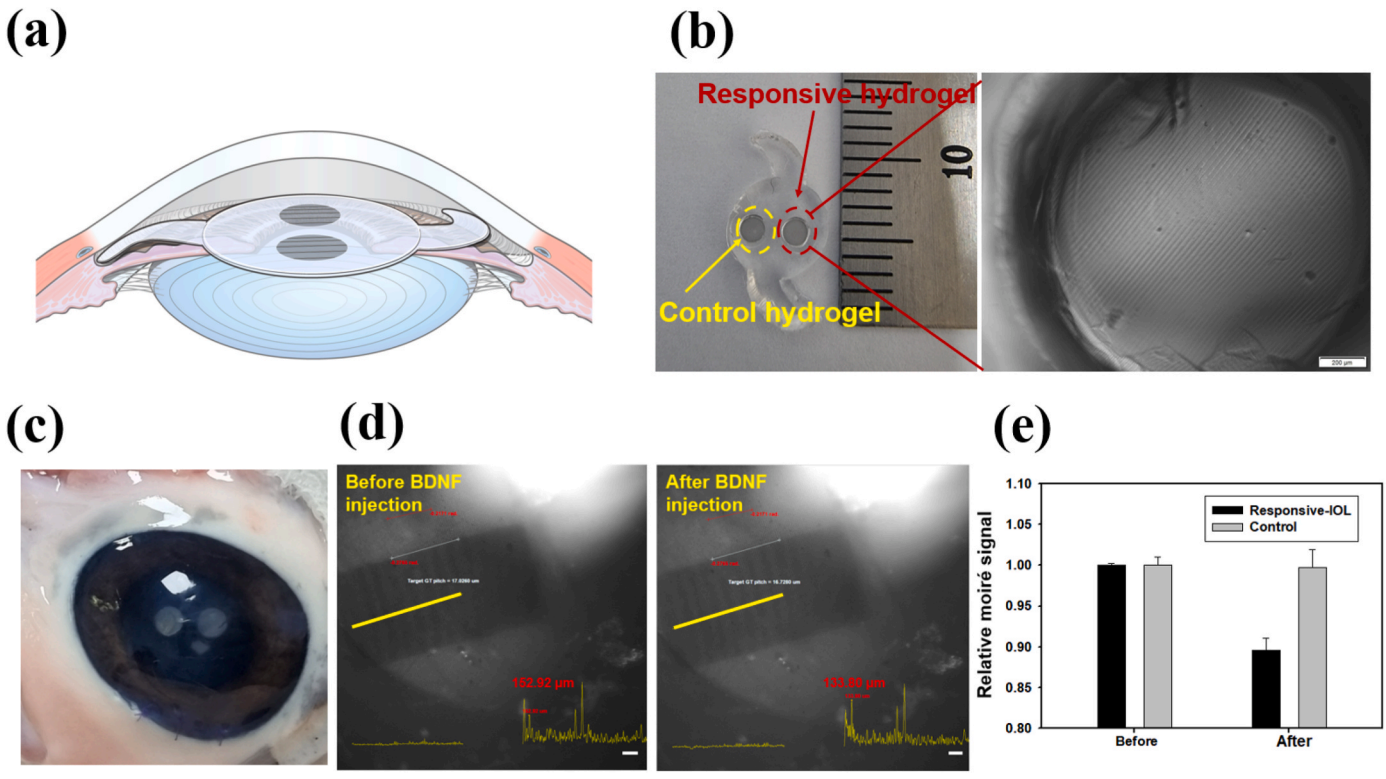

Fig. 6. *Ex-vivo* experiments using BDNF-responsive hydrogel loaded in IOL. (a) Schematic illustration showing PHEMA-based IOL loaded with both control and BDNF-responsive hydrogel gratings, inserted in pig eye. (b) Photo of IOL containing two different hydrogel gratings and optical image of the microgroove pattern on the hydrogel grating. (c) Photo of IOL containing control and responsive hydrogel gratings implanted in pig eye. (d) Optical images change of moiré patterns when BDNF solution (222 nM) is injected in the pig eye. Scale bar: 100 μm. (e) Quantitative analysis of pitch size change of control and BDNF-responsive hydrogels.

Therefore, we do not have any information regarding approval for clinical study, animal study and using human subject.

CRediT authorship contribution statement

Semin Kim: Conceptualization, Methodology, Validation, Formal analysis, Investigation, Data curation, Writing – original draft. **Geehong Kim:** Conceptualization, Software, Investigation, Formal analysis, Data curation, Writing – original draft. **Yong Woo Ji:** Conceptualization, Methodology, Investigation, Formal analysis, Writing – original draft, Writing – review & editing. **Chae-Eun Moon:** Methodology, Investigation. **Yuna Jung:** Investigation. **Hyung Keun Lee:** Conceptualization, Supervision, Writing – review & editing, Project administration. **Jae-Jong Lee:** Conceptualization, Supervision, Writing – review & editing, Project administration. **Won-Gun Koh:** Conceptualization, Supervision, Writing – review & editing, Project administration, Funding acquisition.

Declaration of competing interest

The authors declare that they have no known competing financial interests or personal relationships that could have appeared to influence the work reported in this paper.

Acknowledgement

This work was supported by the National Research Foundation of Korea(NRF) grant funded by the Korea government (Ministry of Science and ICT) (NRF-2017M3A7B4041798, NRF-2021R1A2C4001596, and NRF-2017M3D1A1039289).

Appendix A. Supplementary data

Supplementary data to this article can be found online at https://doi.org/10.1016/j.bioactmat.2022.11.010.

References

[1] T. Miyata, T. Hayashi, Y. Kuriu, T. Uragami, Responsive behavior of tumor-marker-imprinted hydrogels using macromolecular cross-linkers, J. Mol. Recogn. 25 (2012) 336–343, https://doi.org/10.1002/jmr.2190.
[2] A. Gandhi, A. Paul, S.O. Sen, K.K. Sen, Studies on thermoresponsive polymers: phase behaviour, drug delivery and biomedical applications, Asian J. Pharm. Sci. 10 (2015) 99–107, https://doi.org/10.1016/j.ajps.2014.08.010.
[3] H. Cho, S. Jeon, J. Yang, S.Y. Baek, D. Kim, Hydrogel nanoparticle as a functional coating layer in biosensing, tissue engineering, and drug delivery, Coatings 10 (2020) 663, https://doi.org/10.3390/coatings10070663.
[4] S. Merino, C. Martín, K. Kostarelos, M. Prato, E. Vázquez, Nanocomposite hydrogels: 3D polymer–nanoparticle synergies for on-demand drug delivery, ACS Nano 9 (2015) 4686–4697, https://doi.org/10.1021/acsnano.5b01433.
[5] B. Mirani, E. Pagan, B. Currie, M.A. Siddiqui, R. Hosseinzadeh, P. Mostafalu, Y. S. Zhang, A. Ghahary, M. Akbari, An advanced multifunctional hydrogel-based dressing for wound monitoring and drug delivery, Adv. Healthcare Mater. 6 (2017), 1700718, https://doi.org/10.1002/adhm.201700718.
[6] Z. Zhang, Z. He, R. Liang, Y. Ma, W. Huang, R. Jiang, S. Shi, H. Chen, X. Li, Fabrication of a micellar supramolecular hydrogel for ocular drug delivery, Biomacromolecules 17 (2016) 798–807, https://doi.org/10.1021/acs.biomac.5b01526.
[7] N. Sood, A. Bhardwaj, S. Mehta, A. Mehta, Stimuli-responsive hydrogels in drug delivery and tissue engineering, Drug Deliv. 23 (2016) 748–770, https://doi.org/10.3109/10717544.2014.940091.
[8] G. Kim, Y. Jung, K. Cho, H.J. Lee, W.-G. Koh, Thermoresponsive poly(N-isopropylacrylamide) hydrogel substrates micropatterned with poly(ethylene glycol) hydrogel for adipose mesenchymal stem cell spheroid formation and retrieval, Mater. Sci. Eng. C 115 (2020), 111128, https://doi.org/10.1016/j.msec.2020.111128.
[9] H. Ding, B. Li, Z. Liu, G. Liu, S. Pu, Y. Feng, D. Jia, Y. Zhou, Decoupled pH- and thermo-responsive injectable chitosan/PNIPAM hydrogel via thiol-ene click chemistry for potential applications in tissue engineering, Adv. Healthcare Mater. 9 (2020), 2000454, https://doi.org/10.1002/adhm.202000454.
[10] N. Kuroda, Y. Tounoue, K. Noguchi, Y. Shimasaki, H. Inokawa, M. Takano, S. Shinkai, S.-i. Tamaru, Guest-responsive supramolecular hydrogels expressing selective sol–gel transition for sulfated glycosaminoglycans, Polym. J. 52 (2020) 939–946, https://doi.org/10.1038/s41428-020-0341-x.
[11] Y.-T. Tai, W.-N. Chang, D. Wan, Y.-C. Chang, F.-H. Ko, A novel electronic assay based on a sol-gel transition reaction and a thin-film transistor of supramolecular hydrogels to detect alkaline phosphatase activity, Sensor. Actuator. B Chem. 334 (2021), 129591, https://doi.org/10.1016/j.snb.2021.129591.
[12] T. Miyata, N. Asami, T. Uragami, Structural design of stimuli-responsive bioconjugated hydrogels that respond to a target antigen, J. Polym. Sci. B Polym. Phys. 47 (2009) 2144–2157, https://doi.org/10.1002/polb.21812.
[13] T. Miyata, M. Jige, T. Nakaminami, T. Uragami, Tumor marker-responsive behavior of gels prepared by biomolecular imprinting, Proc. Natl. Acad. Sci. USA 103 (2006) 1190–1193, https://doi.org/10.1073/pnas.0506786103.
[14] L.S. Lim, N.A. Rosli, I. Ahmad, A. Mat Lazim, M.C.I. Mohd Amin, Synthesis and swelling behavior of pH-sensitive semi-IPN superabsorbent hydrogels based on poly(acrylic acid) reinforced with cellulose nanocrystals, Nanomaterials 7 (2017) 399, https://doi.org/10.3390/nano7110399.
[15] A. Kim, Swelling properties of hydrogels containing phenylboronic acids, Chemosensors 2 (2014) 1–12, https://doi.org/10.3390/chemosensors2010001.
[16] A.R. Hibbins, P. Kumar, Y.E. Choonara, P.P.D. Kondiah, T. Marimuthu, L.C. Du Toit, V. Pillay, Design of a versatile pH-responsive hydrogel for potential oral delivery of gastric-sensitive bioactives, Polymers 9 (2017) 474, https://doi.org/10.3390/polym9100474.
[17] T. Miyata, N. Asami, T. Uragami, A reversibly antigen-responsive hydrogel, Nature 399 (1999) 766–769, https://doi.org/10.1038/21619.
[18] F. Li, D. Lyu, S. Liu, W. Guo, DNA hydrogels and microgels for biosensing and biomedical applications, Adv. Mater. 32 (2020), 1806538, https://doi.org/10.1002/adma.201806538.
[19] L. Peng, M. You, Q. Yuan, C. Wu, D. Han, Y. Chen, Z. Zhong, J. Xue, W. Tan, Macroscopic volume change of dynamic hydrogels induced by reversible DNA hybridization, J. Am. Chem. Soc. 134 (2012) 12302–12307, https://doi.org/10.1021/ja305109n.
[20] C.-H. Lu, W. Guo, Y. Hu, X.-J. Qi, I. Willner, Multitriggered shape-memory acrylamide–DNA hydrogels, J. Am. Chem. Soc. 137 (2015) 15723–15731, https://doi.org/10.1021/jacs.5b06510.
[21] M. Oishi, K. Nakatani, Dynamically programmed switchable DNA hydrogels based on a DNA circuit mechanism, Small 15 (2019), 1900490, https://doi.org/10.1002/smll.201900490.
[22] M.-K. Shin, Matrix metalloproteinase 9-activatable peptide-conjugated hydrogel-based fluorogenic intraocular-lens sensor, Biosens. Bioelectron. (2020) 162, https://doi.org/10.1016/j.bios.2020.112254.
[23] U. Hasanah, N.D.M. Sani, L.Y. Heng, R. Idroes, E. Safitri, Construction of a hydrogel pectin-based triglyceride optical biosensor with immobilized lipase enzymes, Biosensors 9 (2019) 135, https://doi.org/10.3390/bios9040135.
[24] C. Zhang, M.D. Losego, P.V. Braun, Hydrogel-based glucose sensors: effects of phenylboronic acid chemical structure on response, Chem. Mater. 25 (2013) 3239–3250, https://doi.org/10.1021/cm401738p.
[25] G. Lin, S. Chang, H. Hao, P. Tathireddy, M. Orthner, J. Magda, F. Solzbacher, Osmotic swelling pressure response of smart hydrogels suitable for chronically implantable glucose sensors, Sensor. Actuator. B Chem. 144 (2010) 332–336, 10.1016.j.snb.2009.07.054.
[26] H.R. Culver, M.E. Wechsler, N.A. Peppas, Label-free detection of tear biomarkers using hydrogel-coated gold nanoshells in a localized surface plasmon resonance-based biosensor, ACS Nano 12 (2018) 9342–9354, https://doi.org/10.1021/acsnano.8b04348.
[27] S.G. Shoemaker, A.S. Hoffman, J.H. Priest, Synthesis and properties of vinyl monomer/enzyme conjugates, Appl. Biochem. Biotechnol. 15 (1987) 11–24, https://doi.org/10.1007/BF02798503.
[28] H.M. Yang, B. Yim, B.-H. Lee, Y. Park, Y.G. Kim, J. Kim, D. Yoo, New tool for rapid and accurate detection of interleukin-2 and soluble interleukin-2 receptor α in cancer diagnosis using a bioresponsive microgel and multivalent protein binding, ACS Appl. Mater. Interfaces 13 (2021) 33782–33789, https://doi.org/10.1021/acsami.1c04827.
[29] R. Wu, S. Zhang, J. Lyu, F. Lu, X. Yue, J. Lv, A visual volumetric hydrogel sensor enables quantitative and sensitive detection of copper ions, Chem. Commun. 51 (2015) 8078–8081, https://doi.org/10.1039/C5CC00744E.
[30] Q. Wang, Y. Hu, N. Jiang, J. Wang, M. Yu, X. Zhuang, Preparation of aptamer responsive DNA functionalized hydrogels for the sensitive detection of α-fetoprotein using SERS method, Bioconjugate Chem. 31 (2020) 813–820, https://doi.org/10.1021/acs.bioconjchem.9b00874.
[31] W.L. Murphy, W.S. Dillmore, J. Modica, M. Mrksich, Dynamic hydrogels: translating a protein conformational change into macroscopic motion, Angew. Chem. Int. Ed. 46 (2007) 3066–3069, https://doi.org/10.1002/anie.200604808.
[32] Z. Sui, W.J. King, W.L. Murphy, Dynamic materials based on a protein conformational change, Adv. Mater. 19 (2007) 3377–3380, https://doi.org/10.1002/adma.200700092.
[33] M. Ben-Moshe, V.L. Alexeev, S.A. Asher, Fast responsive crystalline colloidal array photonic crystal glucose sensors, Anal. Chem. 78 (2006) 5149–5157, https://doi.org/10.1021/ac060643i.
[34] Q. Zhu, L. Zhang, K. Van Vliet, A. Miserez, N. Holten-Andersen, White light-emitting multistimuli-responsive hydrogels with lanthanides and carbon dots, ACS Appl. Mater. Interfaces 10 (2018) 10409–10418, https://doi.org/10.1021/acsami.7b17016.
[35] J. Kim, N. Singh, L.A. Lyon, Label-free biosensing with hydrogel microlenses, Angew. Chem. Int. Ed. 45 (2006) 1446–1449, https://doi.org/10.1002/anie.200503102.
[36] J. Kim, N. Singh, L.A. Lyon, Influence of ancillary binding and nonspecific adsorption on bioresponsive hydrogel microlenses, Biomacromolecules 8 (2007) 1157–1161, https://doi.org/10.1021/bm070005p.
[37] H.M. Yang, J.Y. Teoh, G.H. Yim, Y. Park, Y.G. Kim, J. Kim, D. Yoo, Label-free analysis of multivalent protein binding using bioresponsive nanogels and surface

plasmon resonance (SPR), ACS Appl. Mater. Interfaces 12 (2020) 5413–5419, https://doi.org/10.1021/acsami.9b17328.
[38] W. Bai, D.A. Spivak, A double-imprinted diffraction-grating sensor based on a virus-responsive super-aptamer hydrogel derived from an impure extract, Angew. Chem. Int. Ed. 53 (2014) 2095–2098, https://doi.org/10.1002/anie.201309462.
[39] M.I. Lucío, A.H. Montoto, E. Fernández, S. Alamri, T. Kunze, M.-J. Bañuls, Á. Maquieira, Label-free detection of C-Reactive protein using bioresponsive hydrogel-based surface relief diffraction gratings, Biosens. Bioelectron. 193 (2021), 113561, https://doi.org/10.1016/j.bios.2021.113561.
[40] V. Saveljev, S.-K. Kim, J. Kim, Moiré effect in displays: a tutorial, Opt. Eng. 57 (2018), 030803, https://doi.org/10.1117/1.OE.57.3.030803.
[41] F. Porto, Moiré topography: characteristics and clinical application, Gait Posture 32 (2010) 422–424, https://doi.org/10.3390/cancers13153827.
[42] Q. Zhang, H. Xie, Z. Liu, W. Shi, Sampling moiré method and its application to determine modulus of thermal barrier coatings under scanning electron microscope, Opt Laser. Eng. 107 (2018) 315–324, https://doi.org/10.1016/j.optlaseng.2018.04.004.
[43] K. Watanabe, An application of artificial intelligence to diagnostic imaging of spine disease: estimating spinal alignment from moiré images, Neurospine 16 (2019) 697–702, https://doi.org/10.14245/ns.1938426.213.
[44] H.Y. Gong, J. Park, W. Kim, J. Kim, J.Y. Lee, W.-G. Koh, A novel conductive and micropatterned PEG-based hydrogel enabling the topographical and electrical stimulation of myoblasts, ACS Appl. Mater. Interfaces 11 (2019) 47695–47706, https://doi.org/10.1021/acsami.9b16005.
[45] T. Mosmann, Rapid colorimetric assay for cellular growth and survival: application to proliferation and cytotoxicity assays, J. Immunol. Methods 65 (1983) 55–63, 10.1016.0022-1759(00383)90303-4.
[46] T. Yamamoto, T. Kurokawa, J. Ahmed, G. Kamita, S. Yashima, Y. Furukawa, Y. Ota, H. Furukawa, J.P. Gong, In situ observation of a hydrogel–glass interface during sliding friction, Soft Matter 10 (2014) 5589–5596, https://doi.org/10.1039/C4SM00338A.
[47] O. Podrazký, J. Mrázek, J. Proboštová, S. Vytykáčová, I. Kašík, Š. Pitrová, A. A. Jasim, Ex-vivo measurement of the pH in aqueous humor samples by a tapered fiber-optic sensor, Sensors 21 (2021), https://doi.org/10.3390/s21155075.
[48] Y.-T. Tsao, W.-C. Wu, K.-J. Chen, L.-K. Yeh, Y.-S. Hwang, Y.-J. Hsueh, H.-C. Chen, C.-M. Cheng, Analysis of aqueous humor total antioxidant capacity and its correlation with corneal endothelial health, Bioeng. Transl. Med. 6 (2021), e10199, https://doi.org/10.1002/btm2.10199.

Abbreviations

BDNF: brain-derived neurotrophic factor
PDGF: platelet-derived growth factor
IOL: intraocular lens
Con A: concanavalin A
SPR: surface plasmon resonance
AH: aqueous humor
DI: deionized
TGA: thermogravimetric analysis
SEM: scanning electron microscope
CCD: charge-coupled device;
PDMS: polydimethylsiloxane
OVD: ophthalmic viscoelastic device;
LOD: limit of detection
CNS: central nervous system
AA: acrylic acid
AAm: acrylamide
PAAm: poly(acrylamide)
APS: ammonium persulfate
MBAA: Methylenebisacrylamide;
HEMA: 2-hydroxyethyl methacrylate
PHEMA: poly(2-hydroxyethyl methacrylate)
EGDA: ethylene glycol diacrylate
TEMED: N, N, N′, N′-tetramethyl-ethylenediamine
BSA: bovine serum albumin
BSS: Balanced salt solution
FITC: fluorescein isothiocyanate
FITC-BDNF: fluorescein isothiocyanate conjugate brain-derived neurotrophic factor
CEC: cornea endothelial cells
MTT: 3, 4, 5- dimethylthiazol-2-yl)-2–5-diphenyltetrazolium bromide.